Contact Free Monitoring of Cell Density in a Bioreactor with Magnetic Resonance Relaxometry

by

Hans Gaensbauer

B.S., University of Washington (2021)

Submitted to the Department of Electrical Engineering and Computer Science
in partial fulfillment of the requirements for the degree of

MASTER OF SCIENCE IN ELECTRICAL ENGINEERING AND COMPUTER SCIENCE

at the

MASSACHUSETTS INSTITUTE OF TECHNOLOGY

September 2024

Authored by:	Hans Gaensbauer Department of Electrical Engineering and Computer Science July 17, 2024
Certified by:	Jongyoon Han Professor of Electrical Engineering and Computer Science Thesis Supervisor
Accepted by:	Leslie A. Kolodziejski Professor of Electrical Engineering and Computer Science Chair, Department Committee on Graduate Students

Contact Free Monitoring of Cell Density in a Bioreactor with Magnetic Resonance Relaxometry

by

Hans Gaensbauer

Submitted to the Department of Electrical Engineering and Computer Science
on July 17, 2024 in partial fulfillment of the requirements for the degree of

MASTER OF SCIENCE IN ELECTRICAL ENGINEERING AND COMPUTER SCIENCE

ABSTRACT

Frequent, low-latency measurements of bioreactor culture growth are critical for achieving maximum culture efficiency and productivity. Typical cell density and viability measurements are made by removing a sample from the culture, but this approach is both slow and unsuitable for small culture volumes that cannot support frequent destructive sampling. In this work, magnetic resonance relaxometry measurements taken through the walls of the bioreactor tubing are used to monitor the cell density in near real-time. Using intracellular iron as the marker, the system detects variations in cell density in minutes, enabling rapid intervention to save the culture that would be impossible with the once-daily measurements taken by a traditional sampling-based culture analysis system. Given the biochemical importance of intracellular iron, these measurements have the potential to provide phenotypic information on cells without disrupting the bioreactor culture.

Thesis supervisor: Jongyoon Han
Title: Professor of Electrical Engineering and Computer Science

Acknowledgments

I thank Professor Jongyoon Han for his patient support, and for embodying the value of an applications-oriented mindset in research and engineering. The members of the Micro/-Nanofluidics BioMEMS group have made me feel welcome from the moment I started this work, and they regularly inspire me with their dedication, insight, and professionalism. In particular, Do Hyun Park and Alexander Bevacqua's indefatigable efforts to bring the bioreactors online and keep them running made the experiments in this work possible.

I want to thank Daniel DeSantis, Anika Huang, Daniel Sheen, Oliver Trevor, Skylar Dannhoff, and the MIT Radio Society in general for unending free consultation on technical problems, for their unwavering friendship and camaraderie, and for providing the Han Group with a steady stream of very old electronics and test equipment which saw regular use in this project.

I would like to thank Professors Jacob White and Elfar Adalsteinsson for patiently bringing me up to speed with their MRI work and including me in their weekly group debugging sessions, and Joseph Feld and Beth Whittier for their help designing and building the hardware at the heart of our new system.

Finally, I thank my family for their humor and good spirits, and my partner for helping me make it possible to be here. Thank you Willow, Heidi, James and Rebekah.

Contents

List of Figures

Chapter 1

Introduction

1.1 Perfusion Culture and Cell Density Measurement

Biological therapeutic products such as antibodies and viral vectors have many important medical applications, making biomanufacturing a lucrative and expanding field. Many of these products are produced by bioreactor-based cultures of genetically engineered cells. One important example is the Human Embryonic Kidney (HEK) cell culture, which is used to produce viral vectors for cell and gene therapies. During a culture, measurements of the cell density are used to monitor the growth and overall health of the cells. Changes in pH, oxygen saturation, or available nutrients can cause rapid swings in the cell density, and timely action is required to prevent a catastrophic failure of the cell culture. The viable cell density (VCD) is a reasonable proxy for total biologics productivity, offering insight into the bioreactor efficiency and the overall success of the ongoing culture.

VCD is typically measured by removing a sample of cells from the bioreactor which are then analyzed either with cell counting or spectroscopy[1]–[5]. Cell counting often involves either the addition of a stain to improve the signal-to-noise ratio or known concentration of counting beads to account for dilution of the sample during preparation [6], [7]. These preclude the return of the cells to the bioreactor and create a tradeoff between the temporal resolution of VCD measurements and the amount of culture that is lost. For example, the FLEX2 Cell Culture Analyzer from Nova Biomedical, which is widely used for bioprocess monitoring, consumes 400μL of the culture for each cell density and viability measurement. Sample volumes in this range are inconsequential for large-volume bioreactors, but unsuitable for regular measurements on small research bioreactors like the Ambr 250 (Sartorius), which are widely used for process development. While modern systems can perform measurements with sample volumes under 10μL, the sample-to-sample variability increases as the sampling size shrinks[8], [9].

Raman spectroscopy[2], [3], [5], impedance-based VCD estimation[10], and some specialized cell counting techniques[1], [11], [12] have all been applied in-line for sampling-free cell density measurements, but these techniques all require additional wetted hardware that must be cleaned or replaced between runs, increasing the cost and complexity of the bioreactor. Furthermore, changes in the flow dynamics of suspended cell cultures associated with the transitions between different types of tubing can cause cells to form clumps and die, creating

clogs in the bioreactor tubing that can cause the culture to fail. These practical obstacles make it difficult to use VCD as an input for real-time feedback control of the bioreactor, and traditional monitoring methods will struggle to identify problems quickly enough to allow corrective action before they cause the culture to fail.

In this work, we demonstrate a real-time measurement of VCD in a perfusion culture of HEK293 cells through the unmodified tubing of the bioreactor using a low-cost nuclear magnetic resonance (NMR) relaxometer. This approach is, to our knowledge, less invasive than any other technique available because the magnetic fields involved are unaffected by the tubing of the bioreactor as well as the media in which cells are cultured.

1.2 Magnetic Resonance Relaxometry

Magnetic resonance relaxometry measures the rate of decay of excited nuclear populations in a sample, and the hardware required is very similar to that used for magnetic resonance imaging (MRI) or spectroscopy. The sample is placed inside a strong, static magnetic field (referred to as B_0), which creates a small energy preference for nuclei with magnetization that is aligned with the applied field. This creates a net sample magnetization parallel to B_0 that can be caused to precess around B_0 with the application of a small radiofrequency magnetic field, referred to as B_1.

Intracellular paramagnetic Fe^{3+} causes small disruptions to the magnetic fields within cells that drive a faster decay of the observable transverse magnetization of a sample of bioreactor medium as the contributions from different protons lose coherence. The decay of the transverse magnetization, characterized by its time constant T_2 and relaxation rate $R_2 = 1/T_2$ is therefore strongly correlated to the number of cells within the sample. Relaxometry benefits from the natural abundance and high gyromagnetic ratio of the protons in water molecules, and each measurement is analogous to a "single pixel" MRI. However, whereas the goal of MRI is to produce images, relaxometry is a bulk measurement that provides quantitative information about the entire sample volume and its paramagnetic contents.

Because the hardware and working principle of a magnetic resonance relaxometer are almost identical to those used for MRI, this work leans heavily on a large body of recent work on the development of low cost, low complexity MRI systems for point of care applications [13]. Ongoing work at MIT and at the Athinoula A. Martinos Center for Biomedical Imaging has led to cheap, small magnets and readily customizable hardware that provides a very useful reference for the design of a relaxometer [14]–[16]. Because we do not need to resolve spectra and because each measurement is completely nondestructive, the sample volumes can be large. This lowers the requirements for the radio hardware, resulting in a smaller, cheaper system that is easily installed at the site of the bioreactor.

1.3 Magnetic Resonance in Biologics Manufacturing

Previously, R_2 measurements of drugs and vaccines have been used to detect the subtle chemical changes associated with the formation of protein aggregates, freezing, and exposure to oxygen in a purified sample that is free of cells or other background molecules[17]–[22].

This approach has been demonstrated with protein biologics as an in-line quality monitor for bioprocessing[23]. In the purified or single-component samples in these earlier works, the R_2 is sensitive to even subtle changes in the composition or chemical state of the sample. However, similar measurements would not be possible for fluids with significant molecular backgrounds, such as cell culture supernatants.

Recently, our group reported that R_2 is strongly correlated with the cellular Fe^{3+} content, which has, in turn, been correlated with oxidative stress, senescence, and stem cell quality, making benchtop relaxometry with discrete cell samples a well-established quality assurance test[24]–[27]. Since Fe^{3+} is present in virtually all cells, direct R_2 measurements on cell culture solutions (containing cells growing in the culture) will be largely proportional to the number of cells in the sample[28], [29]. This is useful because cell density measurements generalize well to other cell types and culture setups, and the R_2 readings of cells in suspension are dominated by the intracellular iron, which is often the only significant paramagnetic component in biological samples. In the past, several articles described NMR spectroscopy of cultures of mammalian cells, tissue samples, algae, yeast, and chemicals. In some cases, the bioreactor itself is positioned inside the magnet, and the entire culture is measured at once[30], [31], but such an approach is not at all practical with production-scale bioreactors. While several other authors use perfusion systems like the one presented in this work[32]–[35], the use of magnetic relaxometry rather than spectroscopy avoids the need for the expensive magnets used in these publications. More importantly, the high signal-to-noise ratio of a relaxation measurement means each measurement requires only a single scan, allowing meaningful measurements to be made up to every 10 seconds, compared to several minutes to an hour for NMR spectroscopy. To our knowledge, we are the first group to describe magnetic relaxometry-based monitoring of ongoing perfusion-based bioprocessing.

The content of this thesis is largely taken from a manuscript in preparation authored by Hans Gaensbauer, Do Hyun Park, Alexander Bevacqua, and Jongyoon Han. The experiments described here were designed by Jongyoon Han and Hans Gaensbauer. Do Hyun Park and Alexander Bevacqua set up and maintained the perfusion cultures described here, and grew the cells used for calibration.

Chapter 2

MRR Fundamentals

2.1 Magnetic Resonance and Relaxation

The behavior of the nuclear magnetization in the presence of an external field is described by the Bloch equation:

$$\frac{d\vec{M}}{dt} = \gamma(\vec{M} \times \vec{B}) + \begin{bmatrix} -\frac{M_x}{T_2} \\ -\frac{M_y}{T_2} \\ -\frac{M_0 - M_z}{T_1} \end{bmatrix} \tag{2.1}$$

Here, the term $\gamma(\vec{M} \times \vec{B})$ describes the effect of the external magnetic field; without B_1 this reduces to a torque which causes the magnetization to precess around B_0 at the Larmor frequency of $-\gamma B_0$ rad/s. The behavior of the nuclear magnetization in the presence of B_1 is more complex and analysis is usually done in a reference frame that rotates around B_0 at the Larmor frequency. In the rotating frame, the static component of B_0 disappears, and the nuclear magnetization instead precesses around B_1 at $-\gamma B_1$ rad/s [36]. By applying B_1 for $\pi/(2\gamma|B_1|)$ seconds, the magnetization is caused to rotate 90 degrees into a plane perpendicular to B_0. The angle of the rotation caused by a pulsed B_1 is called the flip angle.

After the external B_1 field has been removed, this transverse magnetization persists for as long as the spins are both coherent and still oriented away from their equilibrium alignment with B_0. The rotating magnetic field induces a signal in a receive coil called a free induction decay (FID). Several processes drive the decay of the measurable signal. Variations in the strength of B_0 experienced by nuclei in the sample (from, for example, the presence of dissolved iron) cause the spins to experience slightly different Larmor frequencies, causing the magnetizations from different populations of nuclei to lose coherence and cancel each other out. This process is referred to as spin-spin relaxation or T_2, and it is the parameter in which we are most interested for this work. At the same time, any local magnetic field variations that have energy at the Larmor frequency act to randomize the flip angle, and this also causes a decay back to the equilibrium orientation parallel with B_0 [37]. This process is called spin-lattice or T_1 relaxation.

Importantly, the variations in B_0 from an imperfect magnet also cause nuclei within the

sample to precess at different frequencies. In practice, for the low-cost, permanent magnet systems used in this work, this is a much more significant effect than that from dissolved iron or the cell density, and as a result the signal from a sample of water is observed to decay in 2-5ms, around a thousand times faster than would be predicted by the true 2-3 second T_2 value of water. This decay is referred to as T_2^*, and it makes the estimation of the true T_2 relaxation time from an FID impossible.

To mitigate this, we use a Carr-Purcell-Meiboom-Gill (CPMG) pulse sequence [38]. After the application of a 90 degree pulse for excitation, another pulse is applied to cause a 180 degree flip in the magnetization within the sample. This causes the phase accrued by spins precessing at slightly different frequencies to change sign, and after twice the time between the end of the 90 degree pulse and the center of the 180 degree pulse, the spins realign [39]. This produces an "echo" that can be received by the system.

By repeating many 180 degree pulses after one excitation, we can create a train of echos with decaying amplitudes that represent the true T_2 decay. The time between 180 degree pulses is referred to as the inter-echo time or TE.

2.2 Diffusion and Theoretical Results

An echo train completely reverses the effects of persistent magnetic field variations within a static sample, and this effect is limited only by calibration of the 180 degree flip angle and T_1/T_2 relaxation. For a static sample, this also removes the dependence on magnetic perturbers within the sample and makes the measurement useless for detecting cells. This phenomenon is observable in MRI, where susceptibility artifacts from paramagnetic species are routinely suppressed using fast spin echo sequences very similar to the CPMG experiment used here [40]. However, nuclei that diffuse along a magnetic field gradient between refocusing pulses are not properly realigned because the frequency at which they precess is different before and after the refocusing pulse. Thus, the presence of diffusion provides a new mechanism for the presence of magnetic perturbers to affect the relaxation rate, even in an experiment with refocusing.

A modification to the Bloch equations to include the effects of diffusion was proposed by Torrey in 1959 [41]:

$$\frac{d\vec{M}}{dt} = \gamma(\vec{M} \times \vec{B_0}) + \begin{bmatrix} -\frac{M_x}{T_2} \\ -\frac{M_y}{T_2} \\ -\frac{M_0 - M_z}{T_1} \end{bmatrix} + D\nabla^2\vec{M} \tag{2.2}$$

Torrey's derivation in [41] solves for the attenuation from diffusion after showing that the contributions of diffusion and "classical" T_2 are independent:

$$A(n) = \exp(-\frac{2}{3}nD\gamma^2 \cdot (\nabla\tilde{b_0}(r))^2 \cdot t_1^3) \tag{2.3}$$

Here, n is the echo number, t_1 is one-half the inter-echo time, D is the diffusion constant, γ is the gyromagnetic ratio, and $\tilde{b_0}(r)$ is the deviation from a perfectly even B_0 at point r.

That is, $B_0(r) = \tilde{b_0}(r) + \overline{B_0}$. For a sample where $\nabla\tilde{b_0}(r)$ varies over the sample, the true signal attenuation is the result of integrating (2.2) and the contribution of "classical" T_2 over the sample:

$$A_{T_2}(n) = \iiint_V \exp(-\frac{2}{3}nD\gamma^2 \cdot (\nabla\tilde{b_0}(r))^2 \cdot t_1^3 - \frac{2nt_1}{T_2})dr \tag{2.4}$$

Replacing $\nabla\tilde{b_0}(r)$ with some "effective" average error gradient, we drop the dependence on r and the integral becomes a multiplication. This is insufficient to describe the effect of particle size and distributions, where the full integral needs to be considered. However, for bulk measurements of "regular" samples like the cell-media mixture from a bioreactor this assumption is useful.

The measured relaxation rate is then just the exponent in this expression (using $t = 2nt_1$):

$$A_{T_2}(n) = V \cdot \exp(-\frac{2}{3}nD\gamma^2 \cdot (\overline{\nabla\tilde{b_0}})^2 \cdot t_1^3 - \frac{2nt_1}{T_2}) \tag{2.5}$$

$$\frac{1}{T_{2,eff}} = \frac{1}{T_2} + \frac{1}{3}D\gamma^2(\overline{\nabla\tilde{b_0}})^2 t_1^2 \tag{2.6}$$

Finally, we separate the contributions from B_0 inhomogeneities ($\tilde{b_{0,mag}}$) and intrinsic sample magnetic field variations ($\tilde{b_{0,int}}$):

$$\frac{1}{T_{2,eff}} = \frac{1}{T_2} + \frac{1}{3}D\gamma^2(\overline{\nabla(\tilde{b_{0,int}} + \tilde{b_{0,mag}})})^2 t_1^2 \tag{2.7}$$

This expression illustrates many of the trends that we have seen in calibration data. In particular, in the absence of diffusion ($D = 0$), a CPMG T_2 measurement is not sensitive to magnetic field variations. Diffusion irreversibly mixes spins with different phase accumulations and is responsible for the effect of iron concentration on the T_2 value.

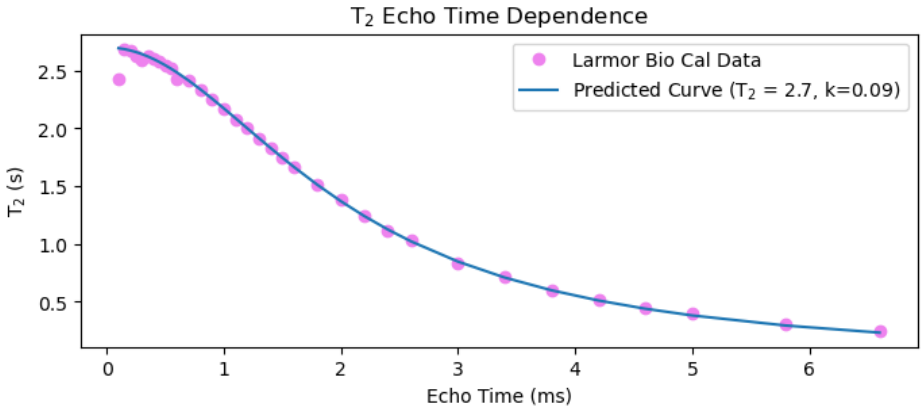

Figure 2.1: Echo time calibration on the Larmor Biosystems MRR with a copper sulfate sample, plotted with the expected result from (2.6). Here, k is the best fit parameter for $\overline{\nabla(\tilde{b_{0,int}} + \tilde{b_{0,mag}})}$. Each point represents a single sample.

The variation in the field from the permanent magnet ($\tilde{b}_{0,mag}$) is likely to be slowly changing, since it is usually caused by imperfect magnet construction like a slight misalignment of the magnet poles. Higher order field variations (that is, those with high spatial frequencies) within the magnet are largely compensated for by the distance between the poles and the sample and the high permeability of the yoke. This results in low field gradients that are almost completely removed by the refocusing pulses. However, the errors caused by microscopic paramagnetic species within the sample ($\tilde{b}_{0,int}$) are necessarily highly localized, producing extremely high gradients through which protons will diffuse during the time between refocusing pulses.

While (2.7) accurately predicts the echo time dependence, we do not expect the parameter k to be linearly related to the paramagnetic species concentration. Furthermore, we expect the T_2 dependence on cell density to take a different form than that for dissolved paramagnetic ions because the perturbers are concentrated within discrete cells. At low cell densities and high intracellular iron concentrations, it may be possible to model the cells as magnetic perturbers using the approaches described in [42]–[47] for highly magnetized spherical particles. However, high resolution diffusion NMR of cells suspended in D_2O suggests that water in cells behaves like bulk water[48], and nitrogen-vacancy based micromagnetometry of cells doped with magnetic nanoparticles shows that the magnetic fields within cells with bound paramagnetic particles are more complicated than the dipole from a single spherical magnetic particle [49]. This suggests that the "highly magnetized" sphere approach will fail to capture significant contributions from the intracellular media and the complicated effects that paramagnetic iron particles within the cells will have on the extracellular medium, particularly at high cell densities. Another complication arises because of the difference of susceptibility between the intra- and extracellular fluid. This causes variations in B_0 at the boundary of the cells, and violates the assumption that the cells and media behave as two distinct components with independent relaxation properties [44]. An estimate of the term $\overline{\nabla(\tilde{b}_{0,int} + \tilde{b}_{0,mag})}$ in (2.7) requires a characterization of not only the magnet quality but also the form of the error in B_0, information about the distribution of paramagnetic species within the sample, and the diffusion within and between the cells.

In practice, this can only be addressed through careful calibration of the instrument on the same cells and media used during a culture, and even then, the measurement is at the mercy of even the slightest changes in any of the variables involved (for example, slow oxidation of some component of the media). For our cultures, where culture conditions change frequently between and even during bioreactor runs, our experience has been that MRR is most useful for answering qualitative questions (are the cells growing? Is their growth faster or slower than usual? and so on). However, in an industrial setting where the operating conditions are carefully controlled, it is relatively simple to measure the relationship between the relaxation time and cell density and use that consistently for calibration.

Chapter 3

Relaxometry Hardware

3.1 Existing MRR Systems

used by our group consists of a KEA 2 console, a custom probe and coil sized for 1mm diameter glass capillary tubes, and a 0.5T permanent magnet. In order to produce measurements for cell quality assessment, several thousand cells are removed from culture and centrifuged, and the experiment is run on the resulting pellet. The magnet is not temperature controlled and variation within 200ms is not considered statistically significant.

Prior to this project, the sensitivity of the instrument was limited by poor probe tuning and the relatively poor noise factor of the preamplifier and receive amplifiers within the spectrometer. The KEA 2 spectrometer is designed for NMR spectrometry and mini-MRI experiments, which are inherently wideband and thus cannot benefit from the narrow bandwidth required for relaxometry.

Recently, work was undertaken to optimize these systems and to identify sources of noise that limit their sensitivity. It was found that all of the probes were out of tune, and a new set of properly tuned probes led to a tenfold improvement in SNR. Combined with smaller coils wound around smaller capillaries, we observed a one-hundred fold improvement in SNR. However, it was also discovered that the receive amplifier and preamplifier have high noise factors (equipment limitations made it impossible to quantify this precisely), and the system has a minimum bandwidth of 100kHz, which is significantly higher than is necessary for relaxometry experiments. The proprietary nature of the system, and the fact that we cannot risk taking it offline due to the many different projects that use it, make further improvements impractical.

In the last year, we have acquired two Larmor Biosystems (Waltham, MA) relaxometers, which have very tight temperature control, high sensitivity, and low noise floors. These tools are more than adequate for the measurements required to monitor a bioreactor but are limited by their proprietary construction, which makes it impossible to program them or modify the magnet assembly.

3.2 Software Defined Relaxometer

In order to develop new probes, pulse sequences, and experiment setups, we needed a functional scanner that can be reconfigured rapidly without expensive hardware changes. To achieve these requirements, we designed a novel instrument for bioreactor monitoring built around a software defined radio (SDR), which shifts the bulk of the signal processing work to a computer.

3.2.1 Hardware

A USRP B210 software-defined radio from Ettus Research (Austin, TX) handles the synthesis and reception of the RF pulses required to perform an experiment, and off-the-shelf, connectorized RF components from Mini-Circuits were used for the analog frontend (AFE).

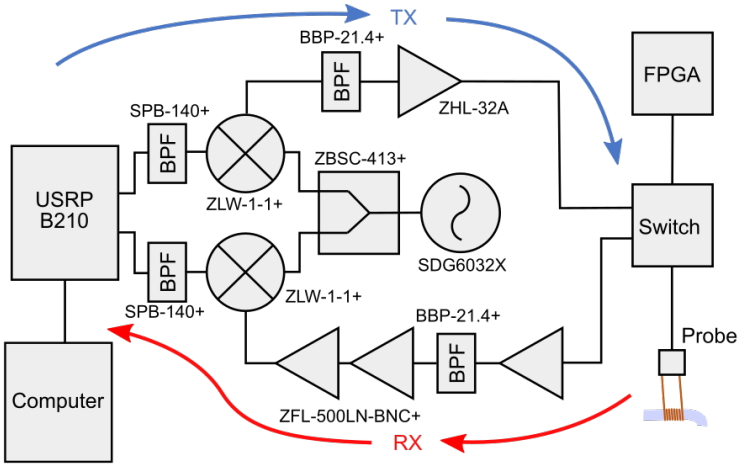

Figure 3.1: A block diagram and photo of the software-defined relaxometer. A power splitter (Mini-Circuits ZBSC-413+) driven by a local oscillator (Siglent SDG6032X), two mixers (Mini-Circuits ZLW-1-1+), and 130-140MHz bandpass filters (Mini-Circuits SPB-140+) are used to shift the frequency range of the radio down to the 20MHz Larmor frequency for our magnet. The 19-23MHz transmit and receive filters (Mini-Circuits BBP-21.4+) reduce the signal bandwidth to 4MHz. The transmit and receive amplifiers are ZHL-32A and ZFL-500LN-BNC+ respectively, from Mini-Circuits.

Because the USRP B210 is not capable of transmitting or receiving at frequencies lower than about 70MHz, it is necessary to shift both the transmit and receive signals up to a 140MHz intermediate frequency outside of the radio. 140MHz was selected because it is relatively free of electromagnetic noise in the environment around the system. Both mixers are driven by the same signal generator (Siglent SDG6032X) to maintain coherence between the transmitter and receiver. The USRP B210 is capable of simultaneous transmission and reception, so it can be used to drive the coil and receive the stimulated RF signal from the sample. After the 140MHz pulses produced by the radio are downconverted to the 22MHz Larmor frequency, they are amplified to around 1 watt and directed through

the transmit/receive switch to the probe. During reception, the signal from the sample is amplified and filtered by two ZFL-500LN-BNC+ amplifiers and two 19-23MHz band-pass filters from Mini-Circuits before being converted to 140MHz again and fed into the radio for detection.

While the USB interface of the USRP B210 is well suited to transmitting and receiving continuously, it is challenging to drive the transmit/receive switch because the general-purpose output pins on the radio are difficult to access quickly through the USB interface. In practice, the shortest inter-echo time that could be achieved with the switch driven by the radio was 3ms. For echo times longer than a few hundred microseconds, diffusion of the water molecules in the sample starts to affect the quality of the refocusing pulses, resulting in shorter-than-expected relaxation curves. To make experiments with smaller inter-echo times possible, the switching patterns are generated by a second FPGA that is triggered by the radio.

3.2.2 Software and Remote Monitoring

In an SDR, most of the signal processing is performed in software rather than by specialized hardware. The radio architecture can be reconfigured by updating the application software, which makes rapid development and experimentation with the system possible. Additionally, because the signals within the system are stored in memory, it is possible to perform extended analysis on individual acquisitions that would be cumbersome or impossible with physical hardware.

In our scanner, the radio is connected to a general purpose computer running JupyterLab, which makes it possible to connect to the instrument remotely to monitor the culture or even trigger new experiments. We use a modified version of the python UHD driver provided by Ettus Research to run CPMG experiments, and the extraction of echo amplitudes and exponential fit for R_2 extraction are performed on the computer. All of the raw radio-frequency data from each experiment is saved to a solid state hard drive, making it possible to retrospectively change the fitting or filtering techniques used for experiments.

3.3 "MR-Core" Replacement System

While the software defined relaxometer system serves extremely well for development and prototyping, its large size and complexity make it poorly suited for use in a laboratory environment. For each of the bioreactor monitoring experiments in which it was used, it had to be installed underneath a biosafety cabinet, a process which took several hours and often resulted in damaged components that would eventually need to be replaced. Furthermore, the high speed USB interface between the SDR and the computer relies on a bloated software stack that would occasionally crash and require a complete system reboot. This happens around once every few weeks of continuous use, which is often enough to cause serious problems for continuous bioreactor monitoring applications.

To address these problems, we developed a system that abandons the commercial radio for a custom hardware implementation. This makes the system much smaller and opens the door to optimizations for our specific needs, like the addition of gradients and improved

analog performance for the Larmor frequencies that we use. We intend to use this system for all future system development work.

3.3.1 Hardware

The MR-Core is built around an Artix-7 FPGA connected to a 500MSa/s digital-to-analog converter and a 125MSa/s analog-to-digital converter. The transmit and receive amplifiers are on a separate daughterboard that allows the analog frontend (AFE) to be optimized without rebuilding the digital system. We use an RJ-45 cable to connect the system to the preamplifier and switch, which are kept separate so that additional amplifiers can be added easily (as the transmit and receive signals are available on separate connectors outside the console).

The FPGA is connected to an ARM microcontroller through the external memory interface, making it possible to access the FPGA with simple memory reads and transfer data to the microcontroller at high speed. The microcontroller is responsible for creating and sequencing experiments, and it also handles high level processing on the received data. The FPGA handles the time-critical task of running pulse sequences, and includes a soft digital demodulator that filters and shifts the 100kHz bandwidth received signal to baseband, significantly reducing the processing overhead for the microcontroller.

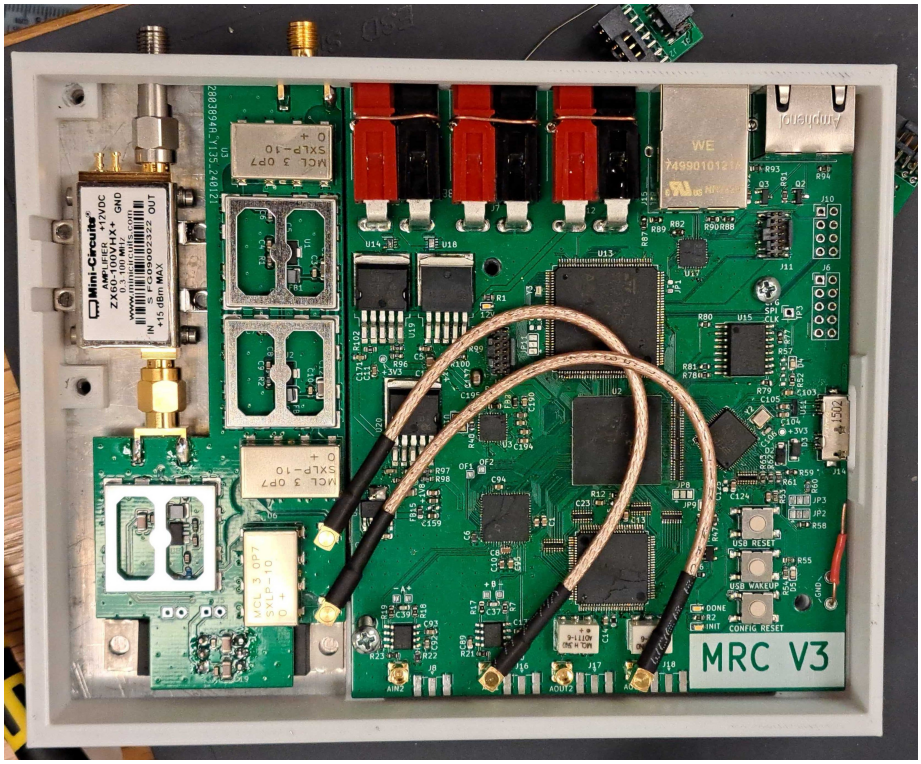

Figure 3.2: The main PCB of the replacement MR console.

As a collaboration with Jacob White's group, an FT601 USB 3.0 to parallel converter is included on the board, which makes it useful for their research as the data acquisition

system for their tabletop MRI systems. This makes it possible to pull full-rate digital data from the FPGA onto an attached computer for debugging and development.

Finally, the new system includes switching drivers for three gradient coils to allow for gradient crushing, slice selection, and rudimentary imaging.

3.3.2 Instruction Set and Sequencer Design

Inspired by the OCRA-MRI system[50], we have designed a custom instruction set for the relaxometer to allow it to run arbitrary sequences. Rather than implement a general purpose computer, we use a significantly reduced instruction set architecture (ISA) that is not Turing complete. Of the only four instructions available, only one (CMD) is functional, and the other three (LSET, JUMP, HALT) manage looping and program flow.

It is highly desirable to be able to update the transmitter amplitude and phase, as well as the values of each of the gradients, in a single clock cycle. Furthermore, to avoid jitter, it should be possible to update each of these outputs on *every* clock cycle. This would typically be done by including the values for the transmitter and gradient parameters as "immediate" fields within the instruction. However, since both the amplitude and phase are 16-bit values, they don't fit inside a 16-bit instruction. To get around this, we observe that most pulse sequences involve only a few different pulse amplitudes (for us, typically only two: one for the 90 degree pulse and one for the 180 degree pulse). During compilation, we extract a list of the unique amplitudes and store them in a separate memory on the FPGA. The command instructions that update the console outputs need only store the index of the correct amplitude and phase, which is extracted from the corresponding memories during sequence execution.

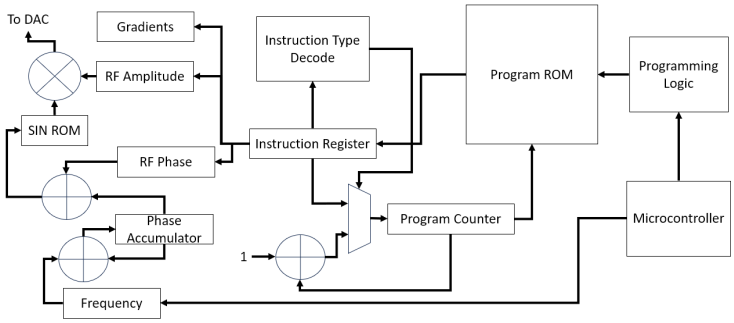

Figure 3.3: A block diagram of the sequencer implemented within the FPGA on the new MR console.

The transmit amplitude and phase, along with a frequency tuning word that is programmed separately (since it does not need to be updated during the experiment) feed a direct digital synthesizer (DDS) on the FPGA which drives the DAC as shown in 3.3.

3.3.3 Digital Downconverter and Receive Chain

While the full 120MSa/s of the ADC is required to cleanly represent the baseband received signal at the Larmor frequency, only around 10kHz of bandwidth around the Larmor fre-

quency contains useful MR information. To enable continuous sample streaming over USB 2.0 and local experiment processing on the STM32, we downconvert and decimate the received signal to 100kSa/s complex data. The DDS, complex multiplier, and decimating filter banks are all implemented on the FPGA. The DDS feeding the complex multiplier uses the same frequency tuning word used by the transmitter DDS, so the transmitted signal is always coherent with the received data. This makes it easy to tune the Larmor frequency on the fly without needing to change the pulse program.

The filter banks are designed in MATLAB, and the calculated taps are brought into Vivado to be used with the FIR filter design tool. The filter topology is shown in 3.4, and features an overall decimation of 1200 with -60dB stopband ripple, far better than could be realized in hardware with the space available.

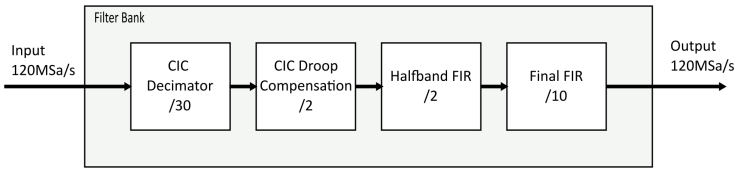

Figure 3.4: The filter topology used by the console receive chain. The filters are designed in MATLAB and the taps are copied into Vivado for implementation as digital FIR/CIC filters.

3.3.4 Software and Pulseq Support

Pulseq is a widely adopted library for designing MR pulse sequences that can be run on many commercial machines. Since it is much easier to develop new pulse sequences using Pulseq than it is to write them in the custom assembly language for the console, we have developed a rudimentary compiler that converts a .seq file into a binary .mrc file that can be loaded into the scanner, and a GCC objdump-style disassembler called mrcdump that will disassemble the machine code for easier debugging.

A central challenge of this effort is the lack of support for loops within Pulseq. CPMG experiments for measuring T_2, which often feature thousands of identical 180 degree pulses, become thousands of repeated lines within the .seq file. This makes the .seq files (and by extension, the compiled .mrc files) very long. Due to limited block RAM available within the FPGA, it is easy to exceed the size of the program memory. We have implemented automatic loop detection and "rolling" in our compiler to allow it to replace repetitive sequences of instructions with assembly loops. After an initial "naive" compilation pass, the compiler searches for repeated blocks of code, and wraps them into loops. This can compress a thousand-line CPMG experiment program to under 30 lines.

To avoid situations where unexpected behavior from the attached computer causes problems for the console, all of the sequencing and control within the console is handled by the STM32. An attached computer can send serial commands such as "calibrate", "load sequence" and "trigger sequence", but all MR functionality is implemented within the console itself. For example, during calibration, the STM32 generates and loads the sequence for

a pulse echo experiment independently, and handles the Fourier transform of the received signal for Larmor frequency detection on-chip.

3.4 Magnet and Coil Assemblies

A uniform, static magnetic field over the sample detection volume is critical for high-quality measurements, especially in our system where no shimming coils are employed to increase uniformity. For relaxometry, where the sample sizes are small and the water signal is easily detected, it is possible to use rare-earth magnets rather than the superconducting magnets typical in MRI and NMR. These permanent magnets have been studied widely for use in portable MRI and bench-top NMR, but they are complicated to design and practically challenging to assemble, and although they are far cheaper and easier to maintain, they are still the most expensive component of the relaxometry system[51]–[54].

3.4.1 Probe Design

For conventional RF measurements, the same solenoid is used to generate B_1 and act as a search coil for receiving the NMR signal. The coil must be tuned to resonate at the Larmor frequency of the sample to maximize sensitivity, and matched to the 50 Ohm impedance of the transmitter and receiver to facilitate power transfer. Ideally, we need to maximize inductance. The signal to noise ratio of the experiment is given in [55]:

$$SNR = K\eta M_0(\frac{\mu_0 Q\omega_0 V_c}{4Fk_B T_c \Delta f})^2 \tag{3.1}$$

K is a correction for coil geometry, η is the volume of the coil that is occupied by the sample, M_0 is the magnitude of the nuclear magnetization, Q is the quality factor, w_0 is the Larmor frequency, F and Δf are the amplifier noise figure and bandwidth, and T_c is the coil temperature.

Because the signal to noise ratio is proportional to Q, a high quality factor is desirable. For small coils wound with magnet wire, the probe can be modeled as a critically loaded series LC resonator, with a quality factor given by [56] :

$$Q_L = \frac{1}{2R_s}\sqrt{\frac{L_c}{C_t}} \tag{3.2}$$

Where R_S is the coil series resistance, L_c is the coil inductance, and C_t is the tuning capacitance. For a fixed resonant frequency given by $\sqrt{LC}$, the Q is maximized by increasing inductance. In NMR and MRI applications, the trade off of a high Q probe is that this increases ringing after a transmitted pulse, and this cuts into the beginning of the FID. For NMR samples with broad linewidths, and for MRI acquisitions with phase or frequency encoding, the FID is typically very short but contains important information about the spectrum or image, so losing hundreds of microseconds at the start of each scan while the coil settles is disadvantageous. This is not a problem for MRR because without gradients, the relaxation signal from biological samples is persists for a long time. The only limiting factor for the optimum inductance are the mechanical constraints associated with probe design and

the increased series resistance caused by increasing the number of turns in the coil, which become very important for microfluidic applications where achieving a high inductance is difficult [57], [58].

The laboratory where the bioreactors are located is a challenging location for sensitive RF work due to significant electrical noise around the Larmor frequency from other equipment. Figure 3.6 shows the spectrum from 14 to 30MHz near the bioreactors. The passband of the receive filters is visible as a lower noise floor below 19 and above 21 MHz, and there are many interfering signals that are not eliminated by the filters because they fall close to the Larmor frequency.

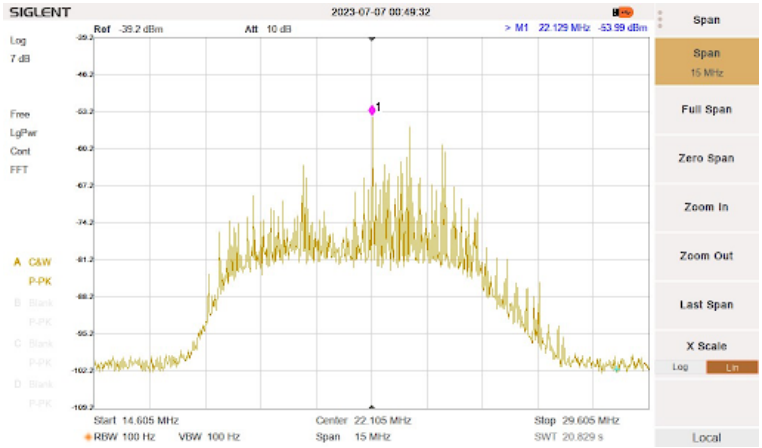

Figure 3.5: The noise spectrum from 14 to 30MHz near the bioreactors.

The probes used in the previous systems ([24]–[27]) use an FR4 PCB to support the coil and capacitors, but they are highly susceptible to noise due to poorly optimized layout. The first set of probes used in this work copied that form factor exactly to ensure compatibility with the old systems, but eliminate the loop in the trace connecting to the coil for superior noise immunity.

More recently, the probe designs have abandoned the PCB format in favor of better shielded designs that are optimized for integration with the bioreactor rather than for ease of use with microhematocrit capillaries. Because the entire bioreactor system must be autoclaved before the culture is started, any part of the probe that is connected to the tubing must be able to survive the autoclave. This is most easily accomplished by winding the coil around the tubing and attaching it to the tuning circuit after autoclaving, however, this adds a considerable amount of complexity to the task of setting up the MRR system because the tuning and matching of the probe must be adjusted after the coil is attached. This is further complicated by the crowded environment around the bioreactors, which makes servicing the instrument difficult and dangerous.

One solution is to push the sample through a set of concentric tubes, capped and connected at one end, as described for NMR applications in [59]. The sample flows down the outer tube to the capped end, where it enters the inner tube and flows back up to the input. A tee at the top provides separate ports for the inner and outer tubes. This assembly can be autoclaved with the bioreactor, and the protruding tube assembly can be inserted into the coil afterward.

Figure 3.6: The original (upper left) and improved (upper right) layouts for the old system probes.

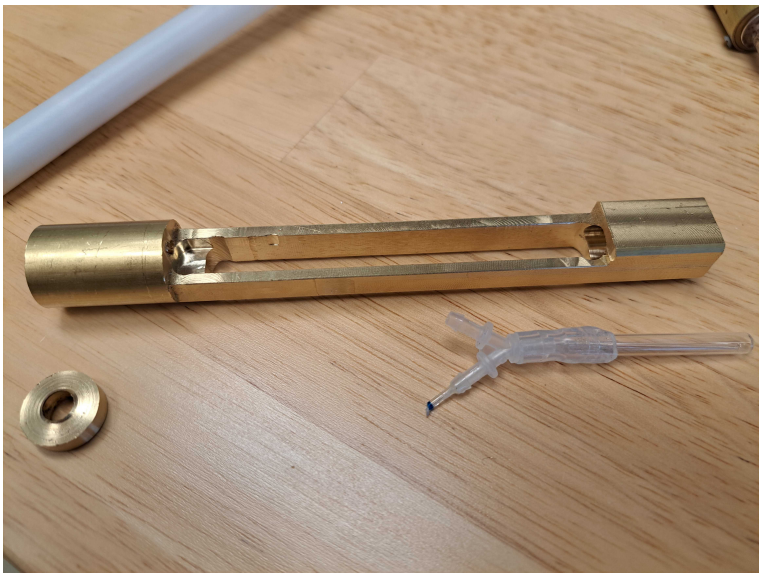

Figure 3.7: The prototype probe with the concentric tubes removed. The brass part is the housing, which contains the coils and the tuning circuit.

In practice, the disrupted flow pattern through this probe caused cells to clump within the probe, and as a result the measured T_2 times showed only the formation and eventual dislodging of the cell clump rather than the more subtle changes from variations in cell density. This geometry is still useful for reaction monitoring applications where clotting within the sample is not an issue.

In fact, even far more straightforward probe geometries that involve an expansion of the tubing to improve the SNR through increased sample volume were found to cause clogging as the cells died and formed clumps. It was thus decided that the only way to guarantee that the addition of the MR system did not have any impact on the operation of the bioreactor was to perform the measurements through the same silicone tubing used to connect different parts of the bioreactor together as shown in Figure 3.8. This is challenging for two reasons. First, for the standard tubing for the bioreactors has a 5mm outer diameter, but only a 0.8mm inner diameter. This means that the fill factor η is 0.04, giving a 96% reduction in SNR. Second, the silicone tubing itself produces a strong MR signal, which swamps the radio and hides the signal from the cells and media. Fortunately, because the silicone has a much shorter T_2 (about 40ms) than the water and cells, after the first 1000 echoes the signal from the tubing is insignificant and can be ignored. To improve the reception of the much weaker water signal after the first thousand echoes, we add 20dB of gain to the receive frontend. As a result, the first part of each scan saturates the receive amplifiers, but after the first 1000 echoes, the signal from the cells and media can be detected. In principle the same result could be achieved using inversion recovery [60, pp. 425-427], but this might bias the multi-component decay signal towards longer decay times from free media and lower the sensitivity to the cells.

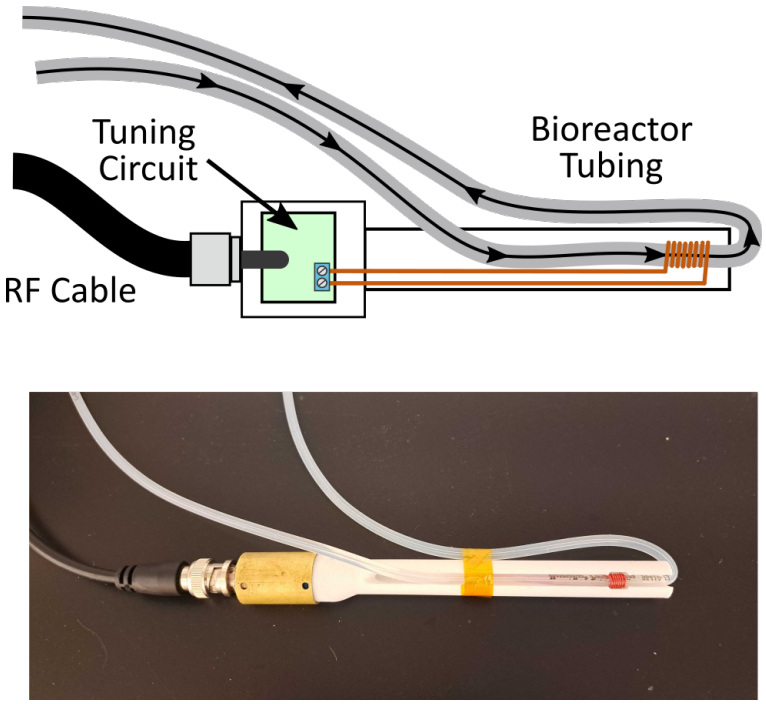

Figure 3.8: The probe assembly used for bioreactor monitoring. The coil is wound around the silicone tubing of the bioreactor, which is supported by a 3D printed frame. The tuning circuit is housed in a shielded brass chamber at the end of the probe.

Finally, for the most recent cultures, it was desirable to take simultaneous measurements of two different bioreactors. To make this possible, an additional RF switch is added at the top of the probe, and another coil is attached next to the first. The system alternates

between the two coils to take measurements. More coils could be added to the same probe assembly and magnet to take measurements at different points in the bioreactor.

3.4.2 Temperature Control

The proton resonant frequency depends linearly on B_0, which drifts significantly with the temperature of the room. While it is possible to calibrate the measurement frequency, each calibration is imperfect and results in some random variation around the resonant frequency. Because the relaxation measurement is affected by even small amounts of frequency offset, the system is calibrated only once at the beginning of the experiment, and the temperature of the magnet is held within 0.001 degrees centigrade throughout the duration of the culture. This keeps temperature-induced variations in the measurement small enough to be insignificant and eliminates the noise created by random variations in calibration. The magnet is a Model 3 NMR Permanent Magnet from SpinCore Technologies Inc. (Gainesville, FL), which is mounted within an aluminum box to eliminate any temperature gradient that might lead to magnetic field inhomogeneity (Figure 3.9). The outside of this box is fitted with 10 small heaters, which are all driven by a large linear amplifier to maintain the magnet temperature at 25.5 degrees for the duration of the experiment. The entire assembly is coated in insulating foam to further isolate it from room temperature.

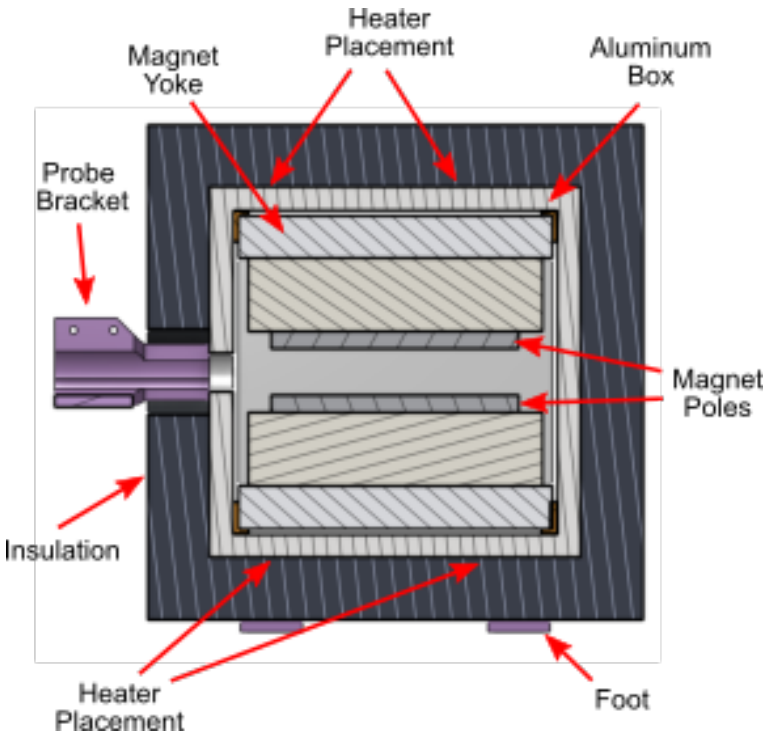

Figure 3.9: The magnet temperature control box and probe assembly. The mag-net is encased in a box made of aluminum channel that distributes the heat from the heaters evenly over the magnet. The temperature sensor is installed below the magnet, and the aluminum channel and heaters are isolated from the room temperature with foam.

Chapter 4

Culture Monitoring

4.1 Offline Measurements

4.1.1 VCD Calibration

A 5-milliliter sample of HEK293 cells from the National Research Council Canada with a viable cell density of 12M cell/ml is first concentrated to 24M cell/ml when half of the supernatant is removed after centrifugation. Samples are prepared by mixing different fractions of the 24M cell/ml suspension and the now cell-free supernatant from the previous step. Each sample is measured in a commercial relaxometer, and the true cell densities are determined afterward using a Flex 2 Cell Analyzer from Nova Biomedical. This experiment is repeated with Chinese Hamster Ovary (CHO) cells from Sartorius GMBH, to confirm that the relationship between the cell density and the sample R_2 generalizes to other cell types.

Figure 4.1 shows examples of this calibration for CHO and HEK293 cells, which are two of the most popular cells used for biomanufacturing.

4.1.2 Cell Viability

While the largest contributor to changes in the R_2 is the cell density, the R_2 varies over the course of the culture in ways that correlate to iron accumulation within the cells. This, in turn, could be used to infer the changes in cells' phenotype in the culture and offer insight into the culture that is not possible with optical cytometry or other cell characterization technologies.

To investigate the sensitivity of R_2 to cell viability, samples of HEK293 cells are prepared with different proportions of heat-killed cells. There is a clear variation in the pellet R_2 with viability (Figure 4.2). For cultures with low cell viability, this will affect the correlation between the cell density and R_2, and the behavior of dead cells will determine whether the R_2 measurements are sensitive to the viable cell density or the total cell density.

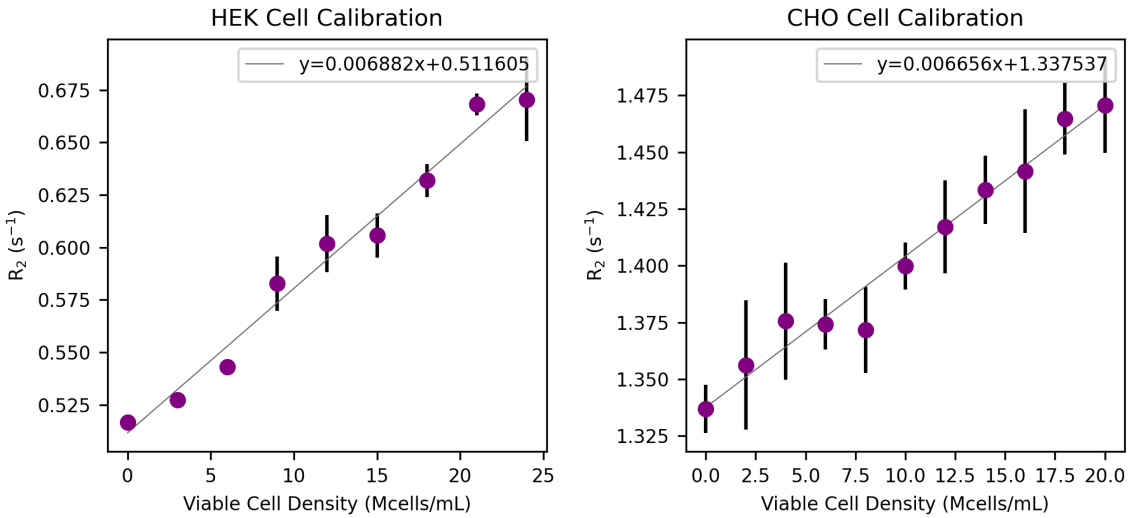

Figure 4.1: R_2 – VCD Calibration of CHO and HEK293 samples suspended in media. 5 µL samples of the 9 different VCDs tested are prepared by diluting a single high-density cell sample with cell free media from the same sample. Each measurement is repeated 3 times, and the standard deviation is shown with error bars. Cell density is correlated with R_2 for both HEK293 and CHO cells

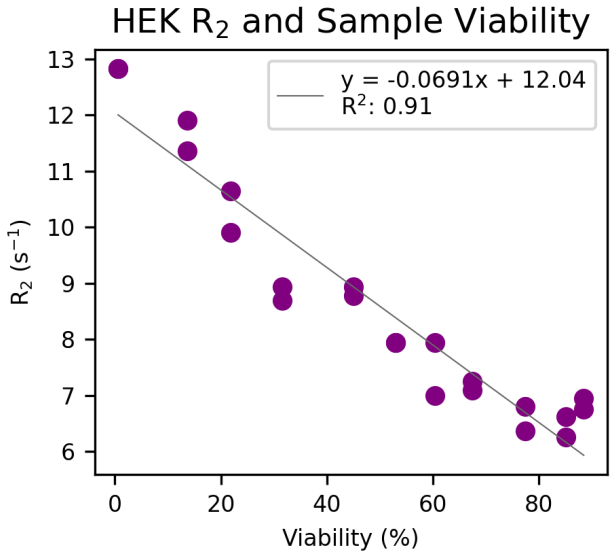

Figure 4.2: The R_2 rate of HEK293 cell pellets with different percent viabilities, created by combining different fractions of living and heat-killed HEK293 cells from the same original sample. For each sample, a 100 µL capillary tube is filled with the cell suspension and centrifuged at 40,000xg for 2 minutes before being measured with an offline relaxometry system provided by Larmor Biosystems.

4.2 Bioreactor Setup

Samples for relaxometry measurements are typically contained in a glass capillary tube that is loaded into the system prior to measurement and discarded afterward. For continuous monitoring, our system combines a relaxometer with a magnet and probe assembly installed around the bioreactor's tubing so that the sample never leaves the bioreactor or encounters the probe (Figure 4.3).

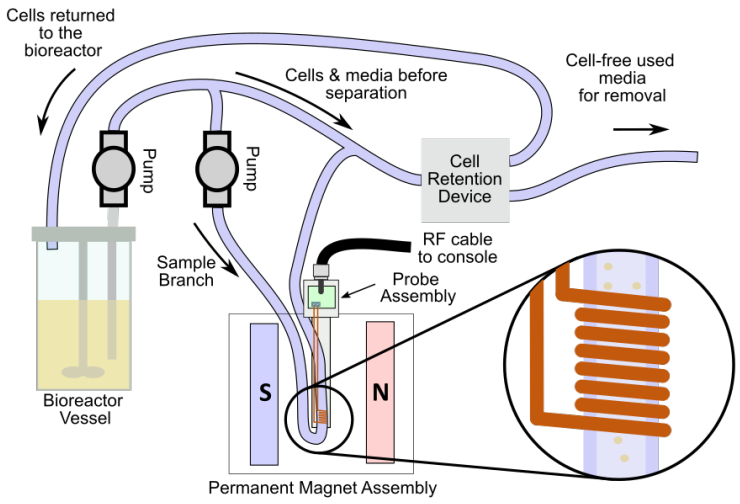

Figure 4.3: The connection between the bioreactor and the relaxometer. The "harvest" line, used to collect cells from the bioreactor, splits and part of the harvest media flows through the magnet and probe before being returned to the bioreactor.

An Applikon miniBio 500ml bioreactor is connected to a series of peristaltic pumps that control the rate of nutrient addition and cell harvesting to maintain optimal nutrient and waste concentrations. The relaxometer is connected to a branch of the tubing that connects the bioreactor to the cell retention device, which sees a continuous flow of cells from the bioreactor. The cells are returned to the same tube in the first two cultures, while in the third culture, they are returned to the retentate stream (in every case, they are pumped back into the bioreactor). The first culture uses HEK293 cells from the University of Massachusetts Chan Medical School, while the second and third use HEK293 cells from the National Research Council Canada. The true cell density and viability are measured once or twice daily using a FLEX2 Cell Culture Analyzer.

4.3 Online Culture Monitoring

Three independent HEK293 cultures were monitored with the online relaxometry system (Figure 4.4). In the first culture (Run 1), the flow through the magnet is stopped for 10 seconds to allow measurements to be taken once every 10 minutes. In the second and third cultures (Runs 2 and 3), the measurement frequency was increased to once every 2 minutes. The raw relaxometry readings are noisy due to the small fraction of the coil volume that is

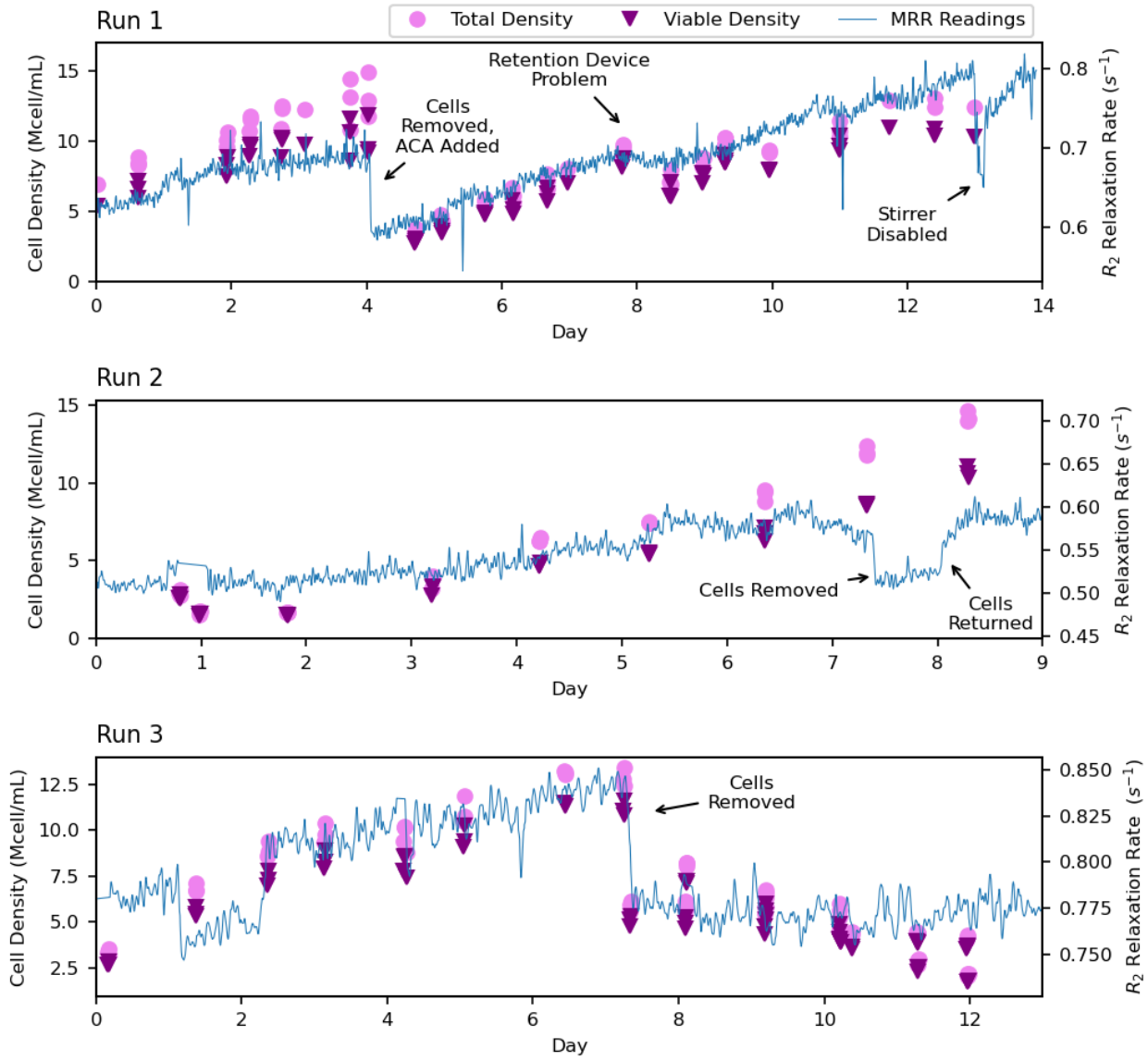

Figure 4.4: Cell density and R2 measurements for three different HEK293 cell cultures. The relaxometry system takes online R2 measurements every 2 minutes, which show good agreement with the measured true viable cell density measured with a Flex 2 cell analyzer from Nova Biomedical through a variety of different perturbations of the culture system.

filled with cells and media and the electrically noisy environment of the laboratory. The raw data is digitally filtered by the computer as it is produced to improve the accuracy of the cell density estimation at the expense of the response time of the relaxometry data. Multiple filters can be used simultaneously to allow for different observations: for example, the slowly changing cell density is best characterized by low cutoff frequencies, while problems like cell clumping, bubbles, and catastrophic failure (as in Run 2) can be detected in minutes without filtering.

In Run 1, most of the cells were removed from the bioreactor on day 4 to simulate a harvest, and an anti-clumping agent (ACA) was added. On day 8, some cells were diverted into the harvest through the cell retention device, causing a loss of cells for several hours. On day 13, the stirrer that keeps the cells in suspension was disabled for an hour accidentally, causing another rapid drop in the cell density. The raw relaxometry estimates over a period of 1 day have a standard deviation of 1.2M cells/ml, compared to 0.8M cells/ml for the cytometry measurements. Before filtering, the drop in cell density following the removal of the cells is apparent after only 10 minutes. With causal lowpass filtering to reduce the standard deviation of cell density measurements over one day to 0.7M cells/ml, this drop is detectable after 40 minutes.

For cell lines that form clumps when they die, almost all of the still-suspended cells are living. When one of these clumps is inside the coil during an experiment, the R_2 is very high, and the measurement is excluded from the cell density curves, implying that in this situation, "normal" measurements do not include dead cells, and the R_2 reflects the viable cell density. After the addition of the anti-clumping agent, dead cells do not form clumps and are therefore included in the measurements, so the R_2 reflects the total cell density. This effect is clearly visible in the data for Run 1.

Additional samples are removed each day and centrifuged to remove the media, which is then measured offline in a relaxometry system provided by Larmor Biosystems (Figure 4.5). This makes it possible to monitor variation in the R_2 caused by variation within the cells themselves, rather than in the cell density. The R_2 rates of the pelleted cell samples did not change significantly, indicating that the measured R_2 signal is mainly determined by the cell number or cell density.

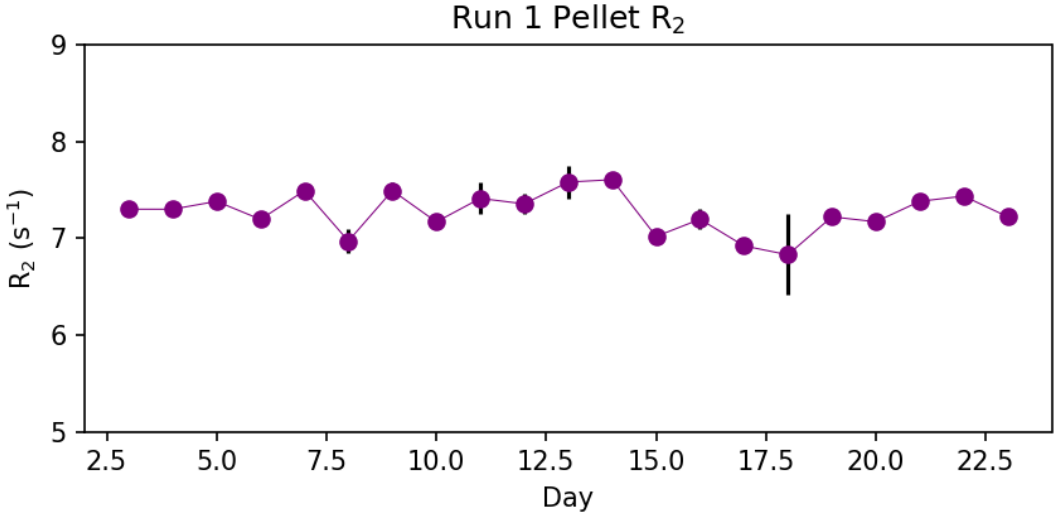

Figure 4.5: R_2 measurements of centrifuged cells from each day during the culture. On each day, we measured two pellets in an offline commercial relaxometer; the average R_2 and standard deviation are shown here.

In Run 2, cells were removed on day 7 and reintroduced on day 8. On day 9, the tubing failed catastrophically, and the bioreactor drained. The catastrophic failure / leak that ended

the second culture was initially detected within two minutes as anomalous readings by the system and confirmed by the absence of the water signal in the raw data from experiments after the leak.

Anomalous readings between the beginning of day 1 and the beginning of day 2 in Run 3 were caused by changes in the flow direction through the tubing leading to the magnet. Cells were removed on day 6.

Chapter 5

Conclusions

This work demonstrates a low-cost system made from off-the-shelf parts for the noninvasive measurement of HEK293 cell density in a perfusion bioreactor. Because the instrument can perform measurements from outside the sterile bioreactor system and no changes need to be made to the bioreactor setup, this approach carries a lower risk and added complexity than other integrated sensors. Discarding the signal from faster relaxing plastics makes it possible to place smaller bioreactors like the Ambr 250 entirely within the magnet so that the cell density can be monitored without any additional pumps or tubing. Furthermore, because this technique is based on the difference in paramagnetic ion concentrations inside the cells rather than a specific feature of HEK293 cell cultures, it is readily applicable to other cell types in other biomanufacturing contexts without the need for additional engineering. The temporal resolution of the filtered R_2 readings is nearly 40 times better than that of traditional cell counting, opening the door to real-time feedback control systems that use the cell density as an input to carefully maintain optimum culture conditions.

More work needs to be done to improve the consistency of measurements between cultures, and to separately measure and characterize the contributions from the media and cell morphology and viability. Since we have already demonstrated that it is possible to switch between two different coils in the same magnet with the same relaxometer, it may be possible to use measurements taken from the harvest line in the bioreactor to estimate the amount of iron in the media. Real time measurements of the media R_2 could further be used to correct the cell suspension measurements for a more accurate estimate of the VCD. In practice, the biggest challenges in expanding the system are related to the complexity of the bioreactor, which must be transported with all of its tubing to the autoclave and back before the culture is started. Using a standardized, autoclavable coil design simplifies the installation of the MR system, and allows us to avoid flip angle calibration between runs. Additionally, new systems are much easier to install into the lab next to the bioreactors due to their higher levels of integration and overall smaller size. Looking beyond our current capabilities, the new system's onboard gradient drivers makes it possible to add "crusher" gradients to suppress excitation from imperfect refocusing pulses, and even to run experiments to estimate the size and diffusion constants of the cells. Finally, we are currently developing coil geometries that will allow this system to work on continuously moving fluids without concern for the flow rate or pump sequencing. This will make it possible to install the system *after* the bioreactor has been set up, without any additional pumps or tubing.

References

[1] A.-L. Heins, M. D. Hoang, and D. Weuster-Botz, "Advances in automated real-time flow cytometry for monitoring of bioreactor processes," *Engineering in Life Sciences*, vol. 22, no. 3-4, pp. 260–278, 2022, ISSN: 1618-2863. DOI: 10.1002/elsc.202100082. (visited on 02/19/2024).

[2] R. M. Santos, P. Kaiser, J. C. Menezes, and A. Peinado, "Improving reliability of Raman spectroscopy for mAb production by upstream processes during bioprocess development stages," *Talanta*, vol. 199, pp. 396–406, Jul. 2019, ISSN: 0039-9140. DOI: 10.1016/j.talanta.2019.02.088. (visited on 04/01/2024).

[3] M.-Y. Li, B. Ebel, C. Paris, F. Chauchard, E. Guedon, and A. Marc, "Real-time monitoring of antibody glycosylation site occupancy by in situ Raman spectroscopy during bioreactor CHO cell cultures," *Biotechnology Progress*, vol. 34, no. 2, pp. 486–493, 2018, ISSN: 1520-6033. DOI: 10.1002/btpr.2604. (visited on 04/01/2024).

[4] A. Tulsyan, G. Schorner, H. Khodabandehlou, T. Wang, M. Coufal, and C. Undey, "A machine-learning approach to calibrate generic Raman models for real-time monitoring of cell culture processes," *Biotechnology and Bioengineering*, vol. 116, no. 10, pp. 2575–2586, 2019, ISSN: 1097-0290. DOI: 10.1002/bit.27100. (visited on 04/01/2024).

[5] D. Yilmaz, H. Mehdizadeh, D. Navarro, A. Shehzad, M. O'Connor, and P. McCormick, "Application of Raman spectroscopy in monoclonal antibody producing continuous systems for downstream process intensification," *Biotechnology Progress*, vol. 36, no. 3, e2947, 2020, ISSN: 1520-6033. DOI: 10.1002/btpr.2947. (visited on 04/01/2024).

[6] J. Kacmar, A. Gilbert, J. Cockrell, and F. Srienc, "The cytostat: A new way to study cell physiology in a precisely defined environment," *Journal of Biotechnology*, vol. 126, no. 2, pp. 163–172, Nov. 2006, ISSN: 0168-1656. DOI: 10.1016/j.jbiotec.2006.04.015. (visited on 02/19/2024).

[7] M. Montes, E. A. Jaensson, A. F. Orozco, D. E. Lewis, and D. B. Corry, "A general method for bead-enhanced quantitation by flow cytometry," *Journal of immunological methods*, vol. 317, no. 1-2, pp. 45–55, Dec. 2006, ISSN: 0022-1759. DOI: 10.1016/j.jim.2006.09.013. (visited on 03/18/2024).

[8] F. W. Kuckuck, B. S. Edwards, and L. A. Sklar, "High throughput flow cytometry," *Cytometry*, vol. 44, no. 1, pp. 83–90, 2001, ISSN: 1097-0320. DOI: 10.1002/1097-0320(20010501)44:1<83::AID-CYTO1085>3.0.CO;2-O. (visited on 02/19/2024).

[9] S. Ramirez, C. T. Aiken, B. Andrzejewski, L. A. Sklar, and B. S. Edwards, "High-throughput flow cytometry: Validation in microvolume bioassays," *Cytometry. Part A: The Journal of the International Society for Analytical Cytology*, vol. 53, no. 1, pp. 55–65, May 2003, ISSN: 1552-4922. DOI: 10.1002/cyto.a.10035.

[10] A. Bergin, J. Carvell, and M. Butler, "Applications of bio-capacitance to cell culture manufacturing," *Biotechnology Advances*, vol. 61, p. 108 048, Dec. 2022, ISSN: 0734-9750. DOI: 10.1016/j.biotechadv.2022.108048. (visited on 05/18/2024).

[11] M. Arnoldini, T. Heck, A. Blanco-Fernández, and F. Hammes, "Monitoring of Dynamic Microbiological Processes Using Real-Time Flow Cytometry," *PLoS ONE*, vol. 8, no. 11, e80117, Nov. 2013, ISSN: 1932-6203. DOI: 10.1371/journal.pone.0080117. (visited on 02/19/2024).

[12] A. Brognaux, S. Han, S. J. Sørensen, F. Lebeau, P. Thonart, and F. Delvigne, "A low-cost, multiplexable, automated flow cytometry procedure for the characterization of microbial stress dynamics in bioreactors," *Microbial Cell Factories*, vol. 12, p. 100, Oct. 2013, ISSN: 1475-2859. DOI: 10.1186/1475-2859-12-100. (visited on 02/19/2024).

[13] S. Fan, Q. Zhou, K.-M. Lei, P.-I. Mak, and R. P. Martins, "Miniaturization of a Nuclear Magnetic Resonance System: Architecture and Design Considerations of Transceiver Integrated Circuits," *IEEE Transactions on Circuits and Systems I: Regular Papers*, vol. 69, no. 8, pp. 3049–3060, Aug. 2022, ISSN: 1558-0806. DOI: 10.1109/TCSI.2022.3187041.

[14] C. Z. Cooley, J. P. Stockmann, T. Witzel, *et al.*, "Design and implementation of a low-cost, tabletop MRI scanner for education and research prototyping," *Journal of Magnetic Resonance*, vol. 310, p. 106 625, Jan. 2020, ISSN: 10907807. DOI: 10.1016/j.jmr.2019.106625. (visited on 10/05/2023).

[15] I. A. Kuang, "Handheld MRI for Point-of-Care and Educational Applications," Thesis, Massachusetts Institute of Technology, Sep. 2023. (visited on 02/23/2024).

[16] I. A. Kuang, "Equivalent-charge-based optimization of spokes-and-hub permanent magnets for hand-held MR imaging," Thesis, Massachusetts Institute of Technology, 2020. (visited on 02/23/2024).

[17] M. B. Taraban, R. A. DePaz, B. Lobo, and Y. B. Yu, "Use of Water Proton NMR to Characterize Protein Aggregates: Gauging the Response and Sensitivity," *Analytical Chemistry*, vol. 91, no. 6, pp. 4107–4115, Mar. 2019, ISSN: 1520-6882. DOI: 10.1021/acs.analchem.8b05733.

[18] M. B. Taraban, T. Ndung'u, P. Karki, K. Li, G. Fung, M. Kirkitadze, and Y. B. Yu, "Analysis of the Adsorbed Vaccine Formulations Using Water Proton Nuclear Magnetic Resonance-Comparison with Optical Analytics," *Pharmaceutical Research*, vol. 40, no. 8, pp. 1989–1998, Aug. 2023, ISSN: 1573-904X. DOI: 10.1007/s11095-023-03528-7.

[19] M. B. Taraban, R. A. DePaz, B. Lobo, and Y. B. Yu, "Water Proton NMR: A Tool for Protein Aggregation Characterization," *Analytical Chemistry*, vol. 89, no. 10, pp. 5494–5502, May 2017, ISSN: 1520-6882. DOI: 10.1021/acs.analchem.7b00464.

[20] M. B. Taraban, Y. Wang, K. T. Briggs, and Y. B. Yu, "Inspecting Insulin Products Using Water Proton NMR. I. Noninvasive vs Invasive Inspection," *Journal of Diabetes Science and Technology*, vol. 16, no. 6, pp. 1410–1418, Nov. 2022, ISSN: 1932-2968. DOI: 10.1177/19322968211023806.

[21] M. B. Taraban, K. T. Briggs, Y. B. Yu, M. T. Jones, L. Rosner, A. Bhambhani, D. M. Williams, C. Farrell, M. Reibarkh, and Y. Su, "Assessing Antigen-Adjuvant Complex Stability Against Physical Stresses By wNMR," *Pharmaceutical Research*, vol. 40, no. 6, pp. 1435–1446, Jun. 2023, ISSN: 1573-904X. DOI: 10.1007/s11095-022-03437-1. (visited on 02/19/2024).

[22] K. T. Briggs, M. B. Taraban, and Y. B. Yu, "Quality assurance at the point-of-care: Noninvasively detecting vaccine freezing variability using water proton NMR," *Vaccine*, vol. 38, no. 31, pp. 4853–4860, Jun. 2020, ISSN: 0264-410X. DOI: 10.1016/j.vaccine.2020.05.049. (visited on 02/19/2024).

[23] M. B. Taraban, K. T. Briggs, P. Merkel, and Y. B. Yu, "Flow Water Proton NMR: In-Line Process Analytical Technology for Continuous Biomanufacturing," *Analytical Chemistry*, vol. 91, no. 21, pp. 13 538–13 546, Nov. 2019, ISSN: 0003-2700. DOI: 10.1021/acs.analchem.9b02622. (visited on 12/07/2023).

[24] W. K. Peng, L. Chen, B. O. Boehm, J. Han, and T. P. Loh, "Molecular phenotyping of oxidative stress in diabetes mellitus with point-of-care NMR system," *npj Aging and Mechanisms of Disease*, vol. 6, no. 1, pp. 1–12, Oct. 2020, ISSN: 2056-3973. DOI: 10.1038/s41514-020-00049-0. (visited on 02/19/2024).

[25] S. S. Thamarath, C. A. Tee, S. H. Neo, D. Yang, R. Othman, L. A. Boyer, and J. Han, "Rapid and Live-Cell Detection of Senescence in Mesenchymal Stem Cells by Micro Magnetic Resonance Relaxometry," *Stem Cells Translational Medicine*, vol. 12, no. 5, pp. 266–280, Mar. 2023, ISSN: 2157-6564. DOI: 10.1093/stcltm/szad014. (visited on 04/15/2024).

[26] J. Z. Y. Tan, J. Chen, D. Roxby, W. H. Chooi, T. D. Nguyen, S.-Y. Ng, S. Y. Chew, and J. Han, "Label-free assessment of differentiation efficiency in iPSC-derived spinal cord progenitor cells via Magnetic Resonance Relaxometry (MRR)," 2022. (visited on 02/19/2024).

[27] J. Han, C. Sing Yian, J. Tan, T. D. Nguyen, and D. Roxby, "Micro Magnetic Resonance Relaxometry (MRR) for Rapid and Non-invasive detection of iPSC Quality and Differentiation," 63/412,640.

[28] M. U. Muckenthaler, S. Rivella, M. W. Hentze, and B. Galy, "A Red Carpet for Iron Metabolism," *Cell*, vol. 168, no. 3, pp. 344–361, Jan. 2017, ISSN: 0092-8674. DOI: 10.1016/j.cell.2016.12.034. (visited on 06/07/2024).

[29] J. Wang and K. Pantopoulos, "Regulation of cellular iron metabolism," *Biochemical Journal*, vol. 434, no. 3, pp. 365–381, Feb. 2011, ISSN: 0264-6021. DOI: 10.1042/BJ20101825. (visited on 06/07/2024).

[30] S. Kubo, N. Nishida, Y. Udagawa, O. Takarada, S. Ogino, and I. Shimada, "A gel-encapsulated bioreactor system for NMR studies of protein-protein interactions in living mammalian cells," *Angewandte Chemie (International Ed. in English)*, vol. 52, no. 4, pp. 1208–1211, Jan. 2013, ISSN: 1521-3773. DOI: 10.1002/anie.201207243.

[31] K. Wachowicz and R. E. Snyder, "A continuous-flow perfusion system for the maintenance and NMR study of small tissue samples in vitro," *Magnetic Resonance Materials in Physics, Biology and Medicine*, vol. 18, no. 1, pp. 35–40, Mar. 2005, ISSN: 1352-8661. DOI: 10.1007/s10334-004-0092-2. (visited on 02/19/2024).

[32] A. J. Oosthoek-de Vries, J. Bart, R. M. Tiggelaar, J. W. G. Janssen, P. J. M. van Bentum, H. J. G. E. Gardeniers, and A. P. M. Kentgens, "Continuous Flow 1H and 13C NMR Spectroscopy in Microfluidic Stripline NMR Chips," *Analytical Chemistry*, vol. 89, no. 4, pp. 2296–2303, Feb. 2017, ISSN: 0003-2700. DOI: 10.1021/acs.analchem.6b03784. (visited on 02/19/2024).

[33] D. Bouillaud, D. Drouin, B. Charrier, C. Jacquemmoz, J. Farjon, P. Giraudeau, and O. Gonçalves, "Using benchtop NMR spectroscopy as an online non-invasive *in vivo* lipid sensor for microalgae cultivated in photobioreactors," *Process Biochemistry*, vol. 93, pp. 63–68, Jun. 2020, ISSN: 1359-5113. DOI: 10.1016/j.procbio.2020.03.016. (visited on 02/20/2024).

[34] R. Gonzalez-Mendez, D. Wemmer, G. Hahn, N. Wade-Jardetzky, and O. Jardetzky, "Continuous-flow NMR culture system for mammalian cells," *Biochimica et Biophysica Acta (BBA) - Molecular Cell Research*, vol. 720, no. 3, pp. 274–280, Jun. 1982, ISSN: 0167-4889. DOI: 10.1016/0167-4889(82)90051-9. (visited on 02/19/2024).

[35] D. Kreyenschulte, E. Paciok, L. Regestein, B. Blümich, and J. Büchs, "Online monitoring of fermentation processes via non-invasive low-field NMR," *Biotechnology and Bioengineering*, vol. 112, no. 9, pp. 1810–1821, 2015, ISSN: 1097-0290. DOI: 10.1002/bit.25599. (visited on 02/20/2024).

[36] I. I. Rabi, N. F. Ramsey, and J. Schwinger, "Use of Rotating Coordinates in Magnetic Resonance Problems," *Reviews of Modern Physics*, vol. 26, no. 2, pp. 167–171, Apr. 1954, ISSN: 0034-6861. DOI: 10.1103/RevModPhys.26.167. (visited on 02/09/2023).

[37] A. Jerschow, *Explorations in NMR Relaxation*, Webinar, Oct. 2023.

[38] S. Meiboom and D. Gill, "Modified Spin-Echo Method for Measuring Nuclear Relaxation Times," *Review of Scientific Instruments*, vol. 29, no. 8, pp. 688–691, Aug. 1958, ISSN: 0034-6748, 1089-7623. DOI: 10.1063/1.1716296. (visited on 04/25/2023).

[39] E. L. Hahn, "Spin Echoes," *Physical Review*, vol. 80, no. 4, pp. 580–594, Nov. 1950. DOI: 10.1103/PhysRev.80.580. (visited on 02/23/2024).

[40] K. Farahani, U. Sinha, S. Sinha, L. C. Chiu, and R. B. Lufkin, "Effect of field strength on susceptibility artifacts in magnetic resonance imaging," *Computerized Medical Imaging and Graphics: The Official Journal of the Computerized Medical Imaging Society*, vol. 14, no. 6, pp. 409–413, 1990, ISSN: 0895-6111. DOI: 10.1016/0895-6111(90)90040-i.

[41] H. C. Torrey, "Bloch Equations with Diffusion Terms," *Physical Review*, vol. 104, no. 3, pp. 563–565, Nov. 1956, ISSN: 0031-899X. DOI: 10.1103/PhysRev.104.563. (visited on 02/19/2024).

[42] R. J. S. Brown, "Distribution of Fields from Randomly Placed Dipoles: Free-Precession Signal Decay as Result of Magnetic Grains," *Physical Review*, vol. 121, no. 5, pp. 1379–1382, Mar. 1961. DOI: 10.1103/PhysRev.121.1379. (visited on 02/21/2024).

[43] B. Issa, "Reduction of T2 Relaxation Rates due to Large Volume Fractions of Magnetic Nanoparticles for All Motional Regimes," *Applied Sciences*, vol. 8, no. 1, p. 101, Jan. 2018, ISSN: 2076-3417. DOI: 10.3390/app8010101. (visited on 09/19/2023).

[44] D. A. Yablonskiy and E. M. Haacke, "Theory of NMR signal behavior in magnetically inhomogeneous tissues: The static dephasing regime," *Magnetic Resonance in Medicine*, vol. 32, no. 6, pp. 749–763, 1994, ISSN: 1522-2594. DOI: 10.1002/mrm.1910320610. (visited on 02/21/2024).

[45] L. T. Rotkopf, L. R. Buschle, H. .-. Schlemmer, and C. H. Ziener, "Influence of diffusion on transverse relaxation rates and phases of an ensemble of magnetic spheres," *Journal of Magnetic Resonance*, vol. 341, p. 107 259, Aug. 2022, ISSN: 1090-7807. DOI: 10.1016/j.jmr.2022.107259. (visited on 09/22/2023).

[46] V. Kenkre, E. Fukushima, and D. Sheltraw, "Simple Solutions of the Torrey–Bloch Equations in the NMR Study of Molecular Diffusion," *Journal of Magnetic Resonance*, vol. 128, no. 1, pp. 62–69, Sep. 1997, ISSN: 10907807. DOI: 10.1006/jmre.1997.1216. (visited on 09/22/2023).

[47] F. T. Kurz, T. Kampf, S. Heiland, M. Bendszus, H.-P. Schlemmer, and C. H. Ziener, "Theoretical model of the single spin-echo relaxation time for spherical magnetic perturbers," *Magnetic Resonance in Medicine*, vol. 71, no. 5, pp. 1888–1895, 2014, ISSN: 1522-2594. DOI: 10.1002/mrm.25196. (visited on 09/22/2023).

[48] E. Persson and B. Halle, "Cell water dynamics on multiple time scales," *Proceedings of the National Academy of Sciences*, vol. 105, no. 17, pp. 6266–6271, Apr. 2008. DOI: 10.1073/pnas.0709585105. (visited on 02/19/2024).

[49] H. C. Davis, P. Ramesh, A. Bhatnagar, A. Lee-Gosselin, J. F. Barry, D. R. Glenn, R. L. Walsworth, and M. G. Shapiro, "Mapping the microscale origins of magnetic resonance image contrast with subcellular diamond magnetometry," *Nature Communications*, vol. 9, no. 1, p. 131, Jan. 2018, ISSN: 2041-1723. DOI: 10.1038/s41467-017-02471-7. (visited on 09/08/2022).

[50] *OCRA MRI - Programming*, https://openmri.github.io/ocra/programming. (visited on 06/16/2024).

[51] K. Chonlathep, T. Sakamoto, K. Sugahara, and Y. Kondo, "A simple and low-cost permanent magnet system for NMR," *Journal of Magnetic Resonance*, vol. 275, pp. 114–119, Feb. 2017, ISSN: 1090-7807. DOI: 10.1016/j.jmr.2016.12.010. (visited on 11/03/2022).

[52] H. Raich and P. Blümler, "Design and construction of a dipolar Halbach array with a homogeneous field from identical bar magnets: NMR Mandhalas," *Concepts in Magnetic Resonance Part B: Magnetic Resonance Engineering*, vol. 23B, no. 1, pp. 16–25, 2004, ISSN: 1552-504X. DOI: 10.1002/cmr.b.20018. (visited on 10/07/2022).

[53] T. Haishi, T. Uematsu, Y. Matsuda, and K. Kose, "Development of a 1.0 T MR microscope using a Nd-Fe-B permanent magnet," *Magnetic Resonance Imaging*, vol. 19, no. 6, pp. 875–880, Jul. 2001, ISSN: 0730725X. DOI: 10.1016/S0730-725X(01)00400-3. (visited on 02/03/2023).

[54] E. Danieli, J. Perlo, B. Blümich, and F. Casanova, "Small Magnets for Portable NMR Spectrometers," *Angewandte Chemie International Edition*, vol. 49, no. 24, pp. 4133–4135, 2010, ISSN: 1521-3773. DOI: 10.1002/anie.201000221. (visited on 10/13/2022).

[55] D. I. Hoult and R. E. Richards, "The signal-to-noise ratio of the nuclear magnetic resonance experiment," *Journal of Magnetic Resonance (1969)*, vol. 24, no. 1, pp. 71–85, Oct. 1976, ISSN: 0022-2364. DOI: 10.1016/0022-2364(76)90233-X. (visited on 02/20/2024).

[56] F. D. Doty, "Probe Design and Construction," in *eMagRes*, R. K. Harris and R. L. Wasylishen, Eds., Chichester, UK: John Wiley & Sons, Ltd, Dec. 2007, emrstm0414.pub2, ISBN: 978-0-470-03459-0. DOI: 10.1002/9780470034590.emrstm0414.pub2. (visited on 10/10/2022).

[57] T. L. Peck, R. L. Magin, and P. C. Lauterbur, "Design and Analysis of Microcoils for NMR Microscopy," *Journal of Magnetic Resonance, Series B*, vol. 108, no. 2, pp. 114–124, Aug. 1995, ISSN: 1064-1866. DOI: 10.1006/jmrb.1995.1112. (visited on 02/20/2024).

[58] V. Badilita, R. Ch. Meier, N. Spengler, U. Wallrabe, M. Utz, and J. G. Korvink, "Microscale nuclear magnetic resonance: A tool for soft matter research," *Soft Matter*, vol. 8, no. 41, pp. 10 583–10 597, 2012. DOI: 10.1039/C2SM26065D. (visited on 09/01/2022).

[59] D. A. Foley, E. Bez, A. Codina, K. L. Colson, M. Fey, R. Krull, D. Piroli, M. T. Zell, and B. L. Marquez, "NMR Flow Tube for Online NMR Reaction Monitoring," *Analytical Chemistry*, vol. 86, no. 24, pp. 12 008–12 013, Dec. 2014, ISSN: 0003-2700. DOI: 10.1021/ac502300q. (visited on 02/21/2024).

[60] E. M. Haacke, R. W. Brown, M. R. Thompson, and R. Venkatesan, *Magnetic Resonance Imaging*, 1st ed. John Wiley & Sons, Ltd, 2014.